The catalytic oxidation of H2S in a stainless steel membrane reactor with separate feed of reactants

Neomagus, H.W.J.P.; Swaaij, W.P.M. van; Versteeg, G.F.

Published in:
Journal of Membrane Science

DOI:
10.1016/S0376-7388(98)00155-0

Publication date:
1998

ELSEVIER

Journal of Membrane Science 148 (1998) 147–160

journal of MEMBRANE SCIENCE

The catalytic oxidation of H_2S in a stainless steel membrane reactor with separate feed of reactants

H.W.J.P. Neomagus, W.P.M. van Swaaij, G.F. Versteeg*

Department of Chemical Engineering, University of Twente, PO Box 217, 7500 AE Enschede, Netherlands

Received 6 October 1997; accepted 8 May 1998

Abstract

The oxidation of H_2S is studied in a membrane reactor with separate feed of reactants. As a novelty in the concept of separate introduction of the reactants, a sintered stainless steel membrane is used, because this type of material is easy to integrate into the reactor, and the catalytic properties of the membrane itself makes the often difficult activation superfluous. The macropore membrane (d_p>1 μm) is characterized in the absence of a pressure difference by diffusion and conversion experiments for determining the porosity to tortuosity ratio. Because the relative large pore diameter of the membrane, Knudsen diffusion is of minor importance and the last important structure parameter of the membrane, B_0, is determined in a permeation experiment.

This membrane reactor is also studied in the presence of a pressure difference over the membrane; a situation where both diffusion and convection affect the overall mass transfer. For this reason, a model based on the dusty gas model (DGM) is used, where the structure parameters are estimated from isobaric conversion and permeation measurements and the physical constants are taken from literature. This model predicts the conversion in the presence of a pressure difference very well, without using fit parameters. Generally, it can be concluded that the performance of this sintered metal membrane reactor can be described and operated equally compared to ceramic membrane reactors with separate feed of reactants. Regarding the fact that there are several other types of sintered metals (e.g. nickel, silver or platinum), this type of membrane reactor seems to be applicable for several other chemical applications.

Keywords: Metal membranes; Membrane reactors; Facilitated transport; Diffusion; Coupled facilitated transport

1. Introduction

In 1990 a novel type of catalytic membrane reactor was presented [1]. It consisted of two chambers separated by a non-permselective membrane (in their study, d_p=300 nm). The membrane was not used for its permselectivity, but acted only as a physical barrier between the reactants which were fed to the opposite sides of the membrane respectively. The reactants diffused into the membrane and a reaction took place at a point where the reactants met. If the reaction rate is fast compared to the mass transfer rate, a small reaction zone will exist at a place determined by the stoichiometry of the reaction, the diffusion coefficients and the concentration of the reactants. Variation of concentration of one of the reactants resulted in a shift of the reaction zone without affecting the

*Corresponding author. Tel.: +31-53-489-4337; fax: +31-53-489-4774; e-mail: g.f.versteeg@ct.utwente.nl

0376-7388/98/$ – see front matter
PII: S0376-7388(98)00155-0

stoichiometry of the reaction. This property makes the reactor attractive for performing reactions that require a strict stoichiometric feed of reactants (e.g. the catalytic reduction of NO_x with ammonia).

Another application of this type of membrane reactor is for kinetically fast, strongly exothermic heterogeneous reaction as suggested by Veldsink et al. [2]. These reactions are often accompanied with severe problems like the formation of explosive mixtures and the occurrence of thermal runaways, with more or less destructive effects. By introducing the reactants on both sides of the membrane, premixing of the reactants is avoided and therefore the above mentioned thermal problems will not occur. Veldsink et al. [2] tested this reactor for the catalytic oxidation of carbon monoxide and the total catalytic oxidation of propane. Saracco et al. [3] showed that by applying a transmembrane pressure difference an increase of the conversion (up to 300% with regard to isobaric operation) could be achieved for the catalytic total oxidation of propane.

This membrane reactor with separate feed of the reactants was always studied for ceramic membranes. However, the use of this type of membranes is hindered and complicated by the activation, i.e. the impregnation of the catalyst which was not reproducible and controllable with regard to the homogeneity and activity. Moreover, the implementation of the membrane in the reactor, which needed a complex ceramic to stainless steel coupling (possibly one of the reasons that ceramic membranes are still not used frequently in the chemical process industry) is still very difficult.

Owing to these two major drawbacks of ceramic membranes, new types of materials for this reactor concept are investigated. A possible alternative is the use of sintered metals, which make the implementation in the reactor much easier. Remaining problems are related to the catalytic properties, however, this is not the issue of the present study. A model reaction was selected for which the metal membrane itself was already catalytically active. A general drawback of this type of material would be rather the large variation in pore radius in the membrane (see Figs. 1 and 2), which possibly makes this material less attractive in the concept of separated feed of reactants. In this work a sintered stainless steel membrane was used. As a model reaction, the iron catalysed oxidation of H_2S was chosen:

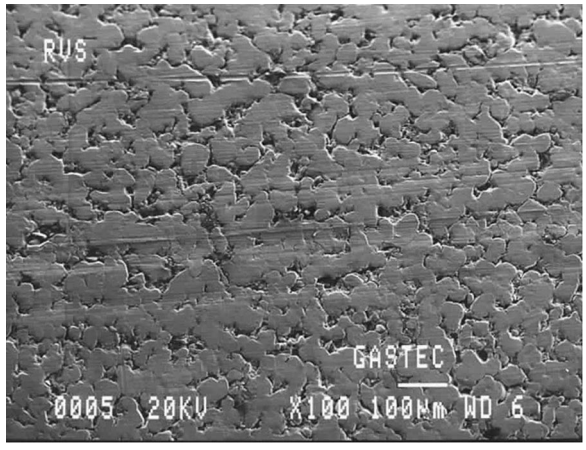

Fig. 1. Surface photo of sintered stainless steel (×100).

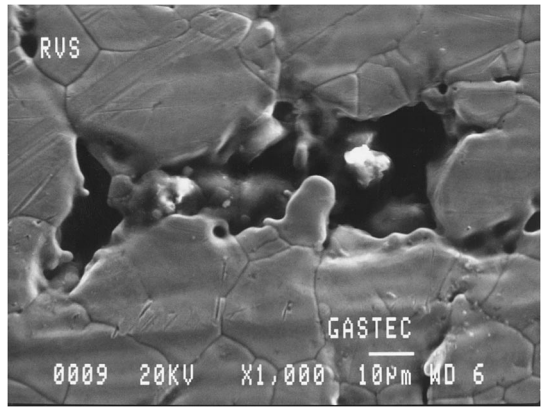

Fig. 2. Surface photo of sintered stainless steel (×1000).

$$H_2S + 1\tfrac{1}{2}O_2 \xrightarrow{Fe} SO_2 + H_2O$$

It is investigated whether this type of material is applicable in the membrane concept with separate feed of the reactants.

2. Theory

The dominating transport phenomenon obtained in macroporous membranes (d_p>0.5 μm) is bulk diffusion and in the case of a pressure difference over the membrane the viscous flow contribution has to be taken into account. Mass transfer in the presence of

a trans-membrane pressure difference cannot be described by a simple Fick model but a specific interaction of diffusion and convection has to be used. For the case of separate feed of reactants, Veldsink et al. [4] demonstrated that the dusty gas model (DGM) based on the Stefan–Maxwell equations is a useful tool.

In Section 2.1 an analytical model is presented for the case of the absence of viscous flow (isobaric operation). The second part deals with a more generally applicable numerical model for predicting the conversion rates in the case where also a trans-membrane pressure difference over the membrane is present. The membrane characterisation has been carried out in the absence- and presence of both a pressure difference and a reaction taking place in the membrane. The four studied situations are schematically summarised in Fig. 3.

2.1. Flux model in the absence of a pressure difference

When there is no pressure difference over the membrane the transport determining phenomenon is diffusion. Because the main free path of both reactants (≈0.065 μm) is much larger than the pore radius (>1 μm) Knudsen diffusion is negligible and molecular diffusion will be the dominant transport mechanism. The situation of absence of pressure difference is studied without (diffusion, Fig. 3(a)) and with (isobaric conversion, Fig. 3(b)) a reaction taking place in the membrane.

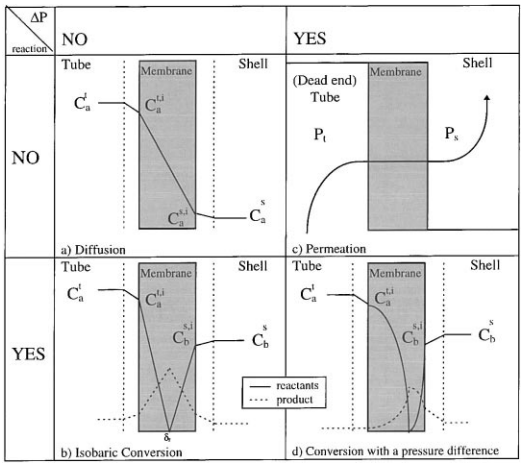

Fig. 3. Summary of experiments carried out with the stainless steel membrane reactor.

2.1.1. Diffusion

Fluxes through a (cylindrical) membrane due to a concentration can be described with the resistances in series model.

In the membrane Fick's law is taken into account:

$$J_{\mathrm{at}} = -D_a \frac{\mathrm{d}c_a}{\mathrm{d}r}. \tag{1}$$

The external mass transfer (from bulk to membrane) on both sides of the membrane can be described with an external mass transfer resistance, where the flux is proportional to the concentration gradient between bulk and interface:

$$J_a = k_{\mathrm{g}}^{\mathrm{t}}(c_a^{\mathrm{t}} - c_a^{\mathrm{t,i}}) \ (\text{tube}), \tag{2a}$$

$$J_a = k_{\mathrm{g}}^{\mathrm{s}}(c_a^{\mathrm{s,i}} - c_a^{\mathrm{s}}) \ (\text{shell}). \tag{2b}$$

The mass transfer coefficients on both sides of the membrane are estimated from the work on heat transfer in annular passages by Lunberg et al. [5]. For obtaining mass transfer coefficients the Chilton–Colburn analogy (Bird et al. [6]) has been used, resulting in:

$$Sh_{\mathrm{t}} = \frac{k_{\mathrm{g}}^{\mathrm{t}} D^0}{d_{\mathrm{t}}} = 3.66, \tag{3a}$$

$$Sh_{\mathrm{s}} = \frac{k_{\mathrm{g}}^{\mathrm{s}} D^0}{d_{\mathrm{s}}} = 6.08. \tag{3b}$$

Integration of Eq. (1) with boundary conditions:

$$c_a(r_{\mathrm{t}}) = c_a^{\mathrm{t,i}}, \tag{4a}$$

$$c_a(r_{\mathrm{s}}) = c_a^{\mathrm{s,i}}, \tag{4b}$$

and taken into account the area of diffusion, results in the following equation for the molar flow of component A:

$$\phi_{\mathrm{mol},a} = \frac{D_a^{\mathrm{eff}}(c_a^{\mathrm{t,i}} - c_a^{\mathrm{s,i}})2\pi L}{\ln(r_{\mathrm{s}}/r_{\mathrm{t}})}. \tag{5}$$

Combining this equation with Eqs. (2a) and (2b) will give

$$\phi_{\mathrm{mol},a} = \frac{2\pi L(c_a^{\mathrm{t}} - c_a^{\mathrm{s}})}{(\ln(r_{\mathrm{s}}/r_{\mathrm{t}})/D_a^{\mathrm{eff}}) + (1/k_{\mathrm{g}}^{\mathrm{t}} r_{\mathrm{t}}) + (1/k_{\mathrm{g}}^{\mathrm{s}} r_{\mathrm{s}})}. \tag{6}$$

The effective diffusion coefficient in Eq. (6) can be calculated from the binary diffusion coefficient multiplied with the quotient of porosity and tortuosity of the porous medium, which is characteristic for the membrane used:

$$D_a^{\text{eff}} = \frac{\epsilon}{\tau} D_a^0, \tag{7}$$

where the binary diffusion coefficients are estimated using the semi-empirical relations of Fuller et al. [7].

$$D_i^0 = \frac{1.013 \times 10^{-7} T^{1.75} (1/M_a + 1/M_b)^{0.5}}{P\left\{ \left(\sum_a v_i\right)^{1/3} + \left(\sum_b v_i\right)^{1/3} \right\}^2}. \tag{8}$$

2.1.2. Isobaric conversion

When an instantaneous reaction takes place in the membrane, profiles as shown in Fig. 3(b) are obtained. For determining the mass transfer rate also Fick's law in the membrane (Eq. (1)) and mass transfer resistances on both sides of the membrane are used, resulting for both components in:

$$\phi_{\text{mol},a} = k_{\text{g}}(c_a^{\text{t}} - c_a^{\text{t,i}}) 2\pi r_{\text{t}} L = \frac{D_a^{\text{eff}} 2\pi L}{\ln((r_{\text{t}} + \delta_{\text{r}})/r_{\text{t}})} c_a^{\text{t,i}}, \tag{9a}$$

$$\phi_{\text{mol},b} = k_{\text{g}}(c_b^{\text{s}} - c_b^{\text{s,i}}) 2\pi r_{\text{s}} L = \frac{D_b^{\text{eff}} 2\pi L}{\ln(r_{\text{s}}/(r_{\text{t}} + \delta_{\text{r}}))} c_b^{\text{s,i}} \tag{9b}$$

regarding the reaction

$$\text{A} + v\text{B} \rightarrow P$$

the molar flow of both reactants are coupled via

$$\nu_b \phi_{\text{mol},a} + (-\phi_{\text{mol},b}) = 0. \tag{10}$$

Combining Eqs. (9a) and (9b) with Eq. (10) and eliminating the location of the reaction plane coordinate (δ_{r}) the following equation for the molar flow of component A can be derived:

$$\phi_{\text{mol},a} = \frac{D_a^{\text{eff}} c_a^{\text{t}} 2\pi L + (D_b^{\text{eff}} c_b^{\text{s}} 2\pi L/\nu_b)}{(D_a^{\text{eff}}/L_{\text{g}}^{\text{t}} r_{\text{t}}) + (D_b^{\text{eff}}/K_{\text{g}}^{\text{s}} r_{\text{s}}) + \ln(r_{\text{s}}/r_{\text{t}})}. \tag{11}$$

If the influence of the external mass transfer resistances is neglected, Eq. (11) can be simplified and rewritten to

$$\frac{\phi_{\text{mol},a}}{c_b^{\text{s}}} \frac{\ln(r_{\text{s}}/r_{\text{t}})}{2\pi L} = \frac{D_b}{V_b} + D_a \frac{c_a^{\text{t}}}{c_b^{\text{s}}}, \tag{12}$$

in which both the effective diffusion coefficient of A and B can be determined very easily.

2.2. Flux model in the presence of a pressure difference

In case of a pressure difference over the membrane, the interaction of viscous flow and diffusion in the porous membrane, has to be taken into account. Therefore an extended model must be used (Veldsink et al. [4]). The mass transfer rates inside the membrane are calculated by solving the mass balance for each component. The flux in the elementary mass balance is calculated with the DGM, where the diffusion coefficients are estimated as given in Section 2.1.1 (see Fig. 4).

If viscous flow affects the mass transfer rate substantially, the simple boundary conditions as shown in Eqs. (4a) and (4b) cannot be used. The concentration gradients in the external film are no longer simply inversely proportional to the mass transfer coefficient, but become a complex function of the fluxes of each component at the membrane interface, as suggested by Bird et al. [6] and also shown in Fig. 4.

The chambers on both sides of the membrane are considered to be ideally mixed and because the overall conversion of the reactants is kept low, the concentration in both compartments are chosen to be the inlet concentration. The viscosity of the gas mixtures is estimated via the method of Chung (Bird et al. [6]).

2.2.1. Permeation

The important structure parameters of the membrane (B_0, K_0 and ϵ/τ) can be derived from permeation measurements of a pure gas through the membrane [8]. For this situation in Fig. 4 the presented model will be reduced to

$$\frac{N_a r_{\text{t}} \ln(r_{\text{s}}/r_{\text{t}}) RT}{|\Delta P|} = \frac{B_0}{\mu} \frac{(P_{\text{t}} + P_{\text{s}})}{2} + \frac{4}{3} K_0 \sqrt{\frac{8RT}{\pi M_a}},$$

for which B_0 and K_0 can be determined, respectively, from the slope and the intercept of the plot of the LHS of Eq. (12) versus the average pressure over the membrane. By assuming non-interconnected and uniform cylindrical pores both the pore radius and the

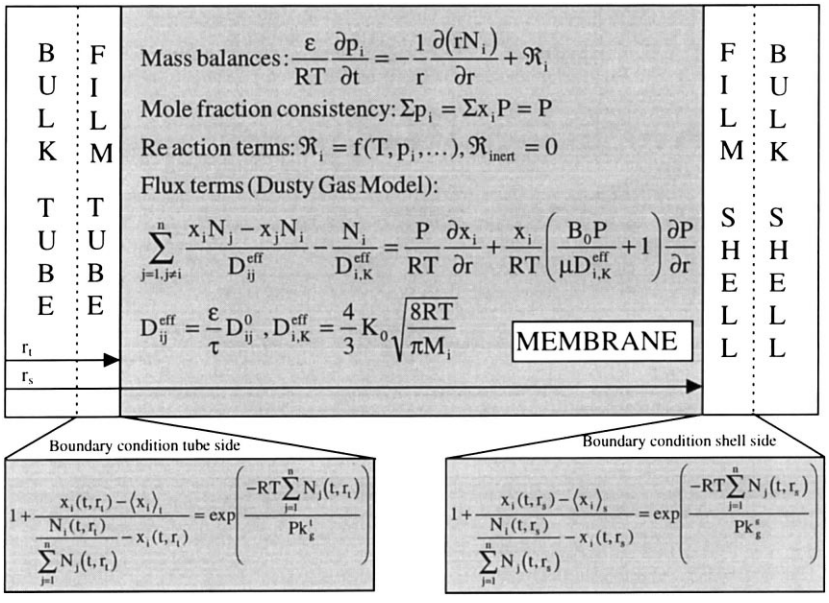

Fig. 4. Schematic representation of the DGM based reactor model.

porosity/tortuosity ratio can be estimated as proposed by Mason and Malinauskas [8] with respectively:

$$\frac{\epsilon}{\tau} = \frac{K_0^2}{2B_0}, \tag{13a}$$

$$r_p = \sqrt{\frac{8B_0}{\epsilon/\tau}}, \tag{13b}$$

$$r_p = \frac{2K_0}{\epsilon/\tau}. \tag{13c}$$

Because the studied membrane has relatively large pores, the Knudsen diffusion is not a substantial transport phenomenon and therefore the estimation of K_0 from the intercept is very inaccurate. Only a global estimation for K_0 and ϵ/τ from permeation measurements can be obtained. The value of K_0 is not so important as cited above and the ϵ/τ ratio can better be examined from experiments carried out without pressure difference as mentioned in Section 2.1.

2.2.2. Reaction in the presence of a trans-membrane pressure difference

If a reaction is taking place in the membrane and there is a pressure difference over the membrane concentration, profiles as shown in Fig. 3(d) are expected. The exact conversions can only be predicted with the DGM in combination with the complex boundary conditions as given in Fig. 4. The various important input parameters are determined from experiments described in Sections 2.1 and 2.2.1 or estimated from literature schematically shown in Fig. 5.

3. Experimental setup

A schematic representation of the experimental setup is shown in Fig. 6(a). Inlet gas mixtures of H_2S (Praxair NV calibration gas) in N_2 (Hoekloos 5.0) and Air (Hoekloos 5.0) in N_2 are introduced into the reactor by four mass flow controllers (Brooks). The mixtures can be fed to the reactor via the tube or the shell side, co- or countercurrently, respectively. In the reactor a cylindrical stainless steel membrane (Krebsöge SIKA-R 0.5 IS, $1<d_p<5$ μm, $\epsilon=0.25$) with a length of 0.025 m and a tube and shell diameter of 0.006 and 0.010 m is welded in the inner tube (see Fig. 6(b)).

The temperature in the reactor is measured and regulated by a Eurotherm and the absolute pressure

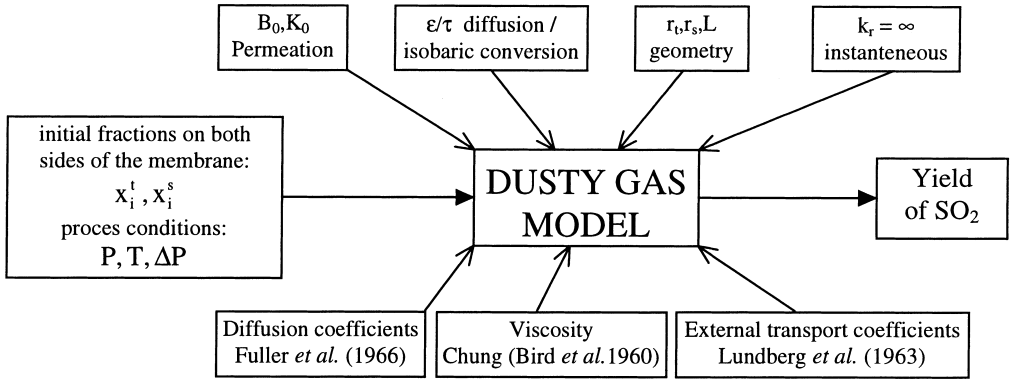

Fig. 5. Schematic representation of the various input parameters for the model.

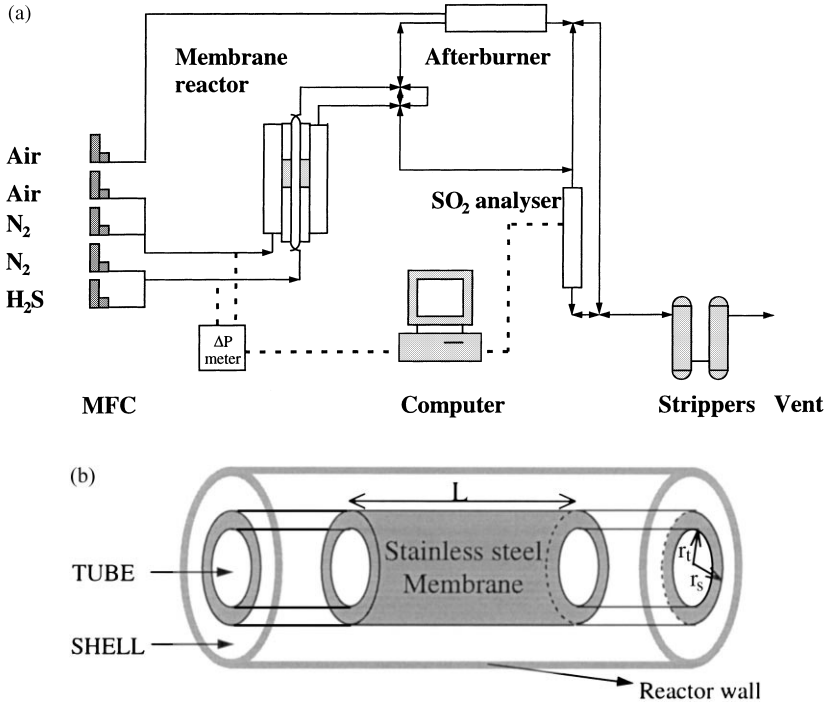

Fig. 6. (a) Experimental set-up; (b) Schematic presentation of the stainless steel membrane reactor.

and pressure difference are controlled by two back pressure regulators. The pressures in both chambers are registered by a digital pressure transducer (Druck) and the pressure difference over the membrane is measured via a pressure difference meter and monitored via a computer. The analysis of the gas streams was carried out by a SO_2 analyser (Maihak Unor 610). The unconverted H_2S was analysed via combustion in an afterburner fed with an excess of air over α-alumina at 850°C to SO_2. After analysing the gas streams were cleaned from H_2S and SO_2 in a stripper before vented.

4. Results and discussion

4.1. Experiments in the absence of a pressure difference

4.1.1. Diffusion

The diffusion experiments are carried out at room temperature and atmospheric pressure. A N_2/H_2S mixture is fed to the tube side (ϕ_v=670 N ml/min, $x_{H_2S} = 0.00244$), while pure nitrogen (ϕ_v=670 N ml/min) is fed to the shell side. The amount of H_2S diffusing through the membrane is related with the effective diffusion coefficient as shown in Eq. (6) and the ϵ/τ ratio can be calculated from this result with Eq. (7). The diffusion experiments are carried out before and after the conversion experiments, carried out at elevated temperature, and are shown in Table 1.

From these results it can be concluded that the effective diffusion coefficients in the membrane were constant during all experiments.

4.1.2. Isobaric conversion

The conversion measurements without a pressure difference over the membrane are visualised in Fig. 7, using the linear form of (with neglecting the external mass transfer coefficients) Eq. (5). In Fig. 7(a) H_2S is fed to the tube side and in Fig. 7(b) it is fed to the shell side respectively. From intercept and slope the effective diffusion coefficients can be derived which are given in the first two rows of Table 2. If the external mass transfer is taken into account according to the correlations of Lunberg et al. [5] the obtained values are presented in the third row of Table 2.

From these results it can be concluded that the external mass transfer has a small influence on the total conversion. The results obtained from these isobaric conversion experiments are consistent, what is demonstrated by the observation that there is no substantial difference between the estimated porosity to tortuosity ratio for hydrogen sulphide and oxygen (0.064 versus 0.061, respectively). Simulation with the DGM (ϵ/τ taken 0.063) showed also very good agreement with the experimental data. Moreover, the distribution of the product SO_2, either to the tube or shell side, is predicted very well, as can be seen in Fig. 7(c).

If the results from diffusion and isobaric conversion are compared, it can be concluded that the obtained ϵ/τ ratio is not completely consistent. A possible explanation for this rather small discrepancy is the inaccuracy in the estimation of the bulk diffusion coefficients. Because the diffusion and conversion experiments are not carried out under the same conditions an under- or overestimation of the bulk diffusion coefficient, directly influences the obtained value of ϵ/τ (see Eqs. (7) and (8)). As the temperatures of the conversion experiments in the presence of a pressure difference (Section 4.2.2) are the same as those in the isobaric conversion experiments, the obtained ϵ/τ ratio from these experiments (Table 2) are used in this situation.

Table 1
Results of diffusion experiments

	Temperature (K)	Pressure (bar)	$D^{eff}_{H_2S}$ (m^2/s)	ϵ/τ
Before	294	1.06	1.29×10^{-6}	0.072
After	293	1.05	1.30×10^{-6}	0.071

Table 2
Results of isobaric conversion experiments (T=573 K, P=1.1 bar)

	$D^{eff}_{H_2S}$ (m^2/s)	ϵ/τ	$D^{eff}_{O_2}$ (m^2/s)	ϵ/τ
H_2S tube	3.45×10^{-6}	0.065	2.83×10^{-6}	0.053
H_2S shell	2.96×10^{-6}	0.048	3.20×10^{-6}	0.052
With k_g resistance	3.41×10^{-6}	0.064	3.27×10^{-6}	0.061

4.2. Experiments in the presence of a pressure difference

4.2.1. Permeation

The permeation measurements for determining the structure parameters are given in Fig. 8, where the left side of Eq. (12) is plotted against the average pressure inside the membrane. B_0 and K_0 are determined from the slope and intercept. It can be seen from the results, which are summarised in Table 3, that the permeability coefficient (B_0) remained constant. B_0 has only raised marginally, which is possible due to the sintering of the smallest (dead-end) pores, resulting in an averaged higher pore radius. The determination of K_0 is, because of the large extrapolation, not very accurate, but because of the minor influence of the Knudsen diffusion on the overall transport rate also not very important. Owing to the high inaccuracy of the values

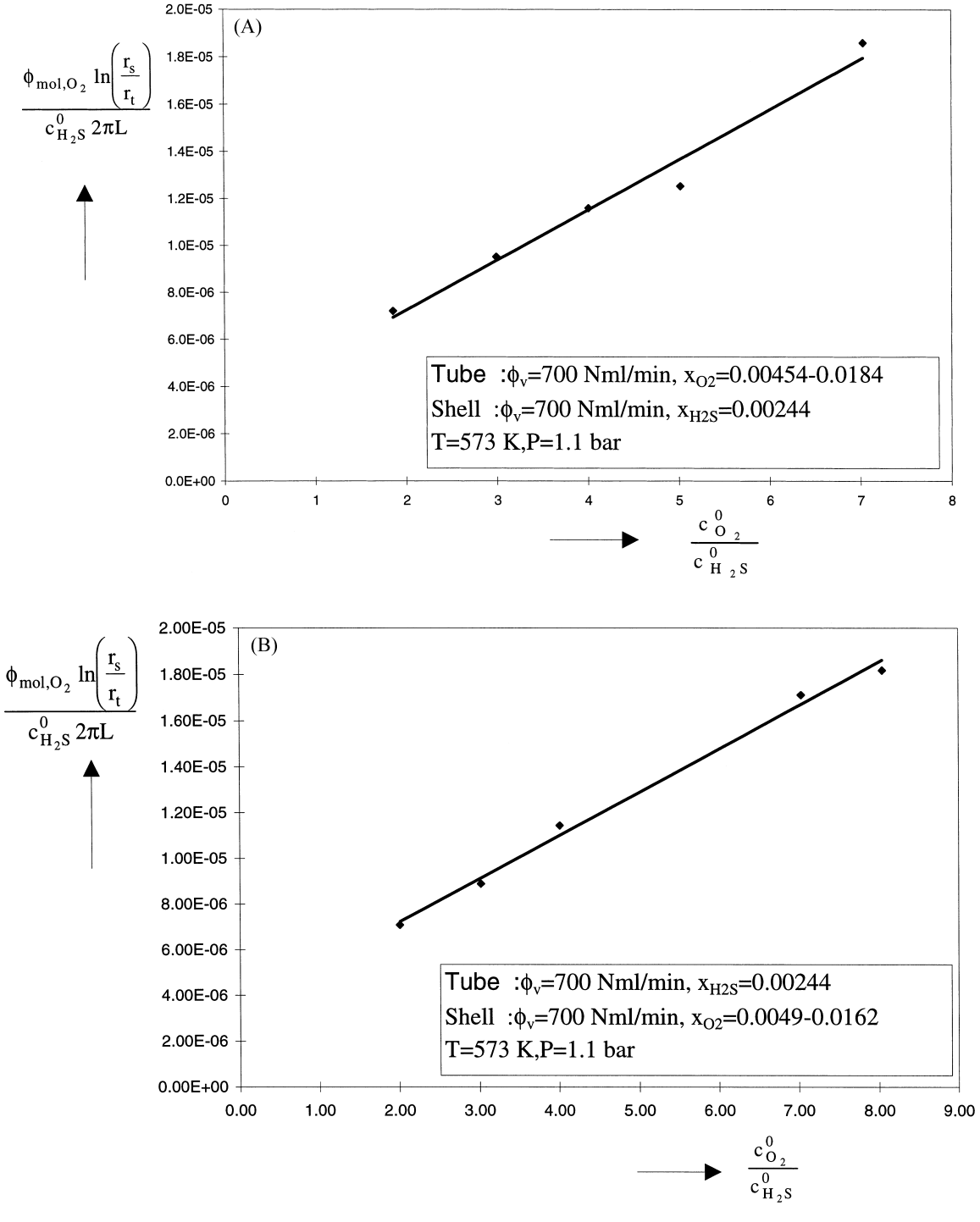

Fig. 7. (a) Estimation of effective diffusion coefficients in the membrane with neglecting the external mass transfer. Oxygen is fed to the tube side and hydrogen sulphide to the shell side, (b) Estimation of effective diffusion coefficients in the membrane with neglecting the external mass transfer. Oxygen is fed to the shell side and hydrogen sulphide to the tube side, (c) Comparison of experimental conversion with the prediction of DGM (ϵ/τ=0.063, for experimental conditions see Fig. 5(a)).

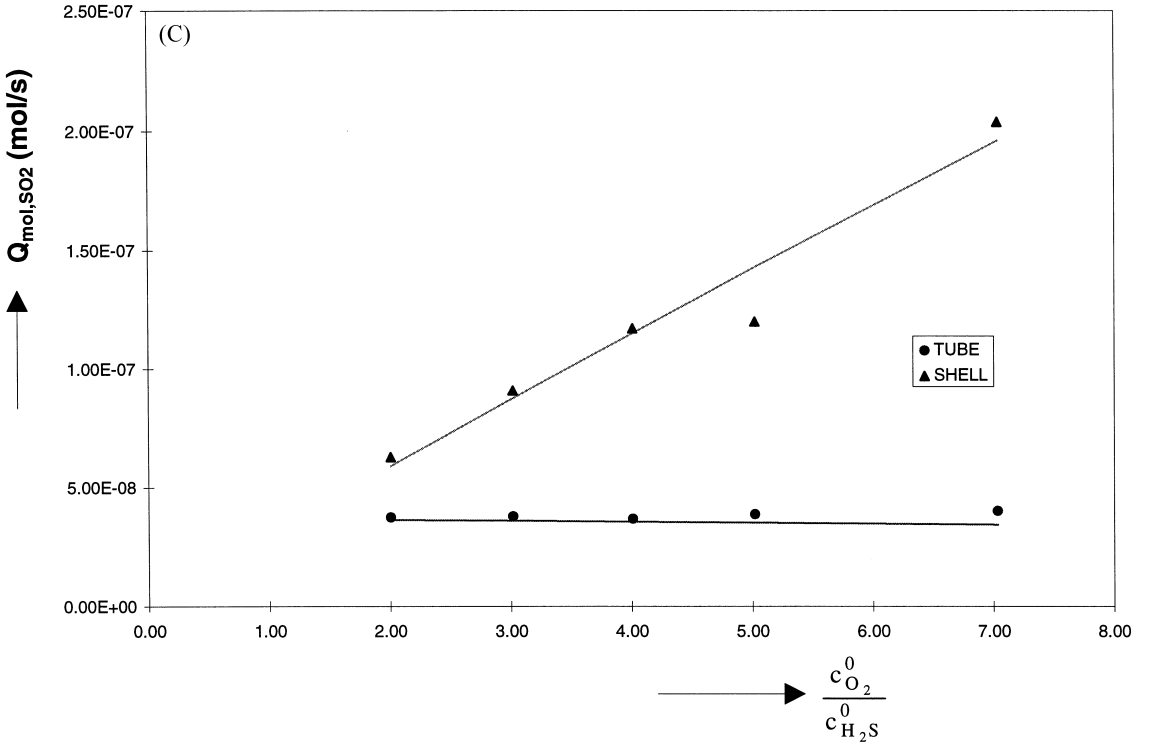

Fig. 7. (Continued)

Table 3
Results of permeation experiments

	K_0 (m)	B_0 (m^2)
Before conversion experiments	1×10^{-7}	6.5×10^{-14}
After conversion experiments	3×10^{-8}	6.7×10^{-14}

obtained for K_0, it is not realistic to estimate the ϵ/τ-ratio from these experiments.

4.2.2. Conversion in the presence of a pressure difference

With all the characteristics obtained from these experiments without a pressure difference over the membrane and the permeation measurements all the characteristics of the membrane are known, and the influence of a pressure difference over the membrane in combination with a reaction inside the membrane can be predicted with the DGM schematically visualised in Fig. 5.

In Fig. 9 the formation of SO_2 is plotted against the pressure difference over the membrane (with the high pressure on the shell side). As can be seen in this figure, the conversion is substantially increased with the pressure difference. Also the distribution of the product is affected and favoured to the (low pressure) tube side, due to a shift of the reaction plane in the membrane. This shift is visualised in Fig. 10 where the calculated fraction profiles are plotted for a situation without pressure difference (Fig. 10(a)) and with a pressure difference of 36.4 mbar (Fig. 10(b)). The model predictions (lines in Fig. 9) are in good agreement with the experiments and the conclusion can be drawn that sintered stainless steel membranes can be characterised with similar experimental techniques as used for ceramic membranes. The influence of the ϵ/τ-ratio on the outcome of the simulation is given in Fig. 11, in which the total molar flow of SO_2 is calculated for three different ϵ/τ-ratios: 0.053, 0.063 and 0.073, respectively. From this figure it can be concluded that the value of ϵ/τ has a substantial

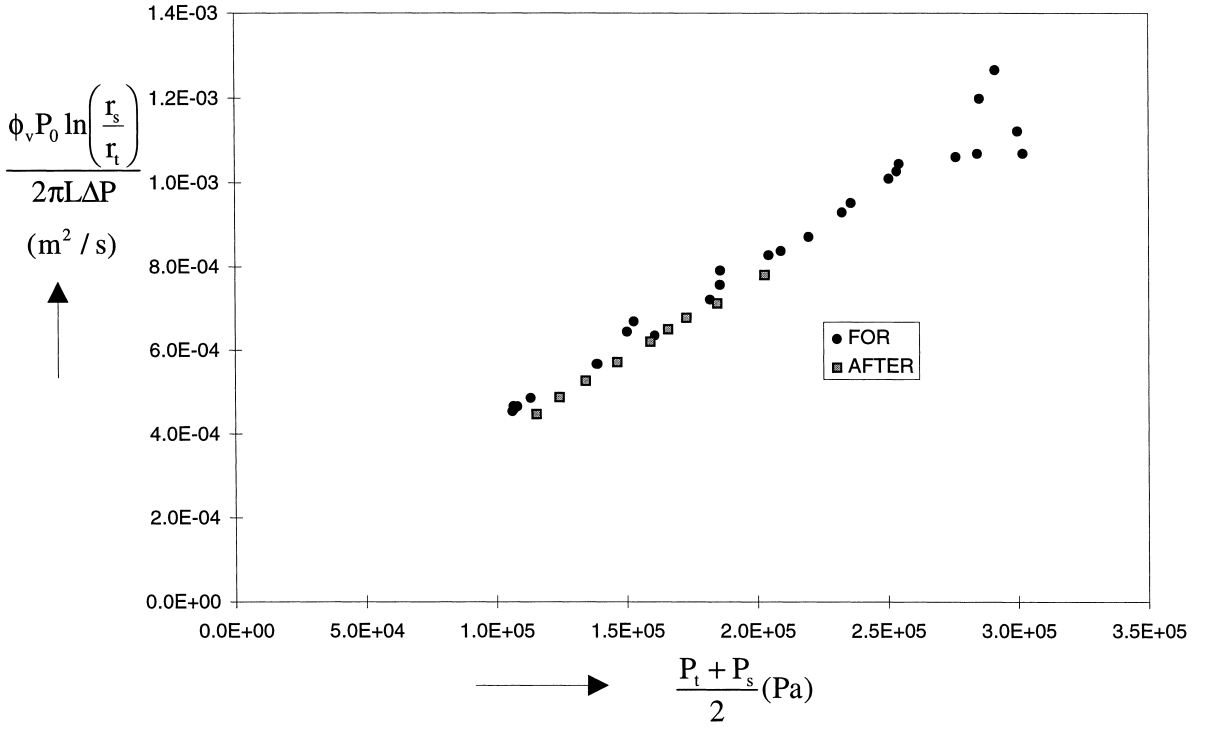

Fig. 8. Permeation experiments with nitrogen at T=294 K.

influence on the calculated SO_2 flow. With increasing the pressure difference over the membrane, the discrepancies between the outcomes of the simulations are decreasing, because the influence of diffusion becomes less important. Furthermore, the value of ϵ/τ of 0.063, as determined from the isobaric conversion experiments (Section 4.1.2), gives a satisfactory agreement between experiments and simulations, as mentioned before, however a slightly higher value of ϵ/τ would improve the comparison. Also this indicates that the diffusion experiments (Section 4.1.1), where a value of 0.071 has been measured, are in line with the present results.

5. Discussion with regard to the applicability of sintered stainless steel

Because the membrane itself has been used as the catalyst, a homogeneously active membrane was guaranteed, and the applicability of the membrane principle of separate feed of reactants is demonstrated satisfactorily. If the pore radius is calculated with Eq. (13c), using the B_0 and ϵ/τ-ratio determined by the permeation- and isobaric conversion measurements, respectively, a pore radius of 2.9 μm is found. This result is in good agreement with the value of 3 μm given by Krebsöge in their product information [9]. Although this same product information also gives a pore radius distribution of 1–5 μm it is demonstrated that this rather large pore radius distribution has no detectable effects on the performance of a sintered stainless steel membrane reactor with the concept of separate feed of reactants. Keeping in mind that there are other types of sintered metals (e.g. nickel, silver or platinum), the membrane concept in combination with these materials opens the door to several other applications.

6. Conclusions

A membrane reactor based on sintered stainless steel is an attractive application for the concept of separated feed of reactants. The membrane is easily integrated into the reactor and because the catalytic

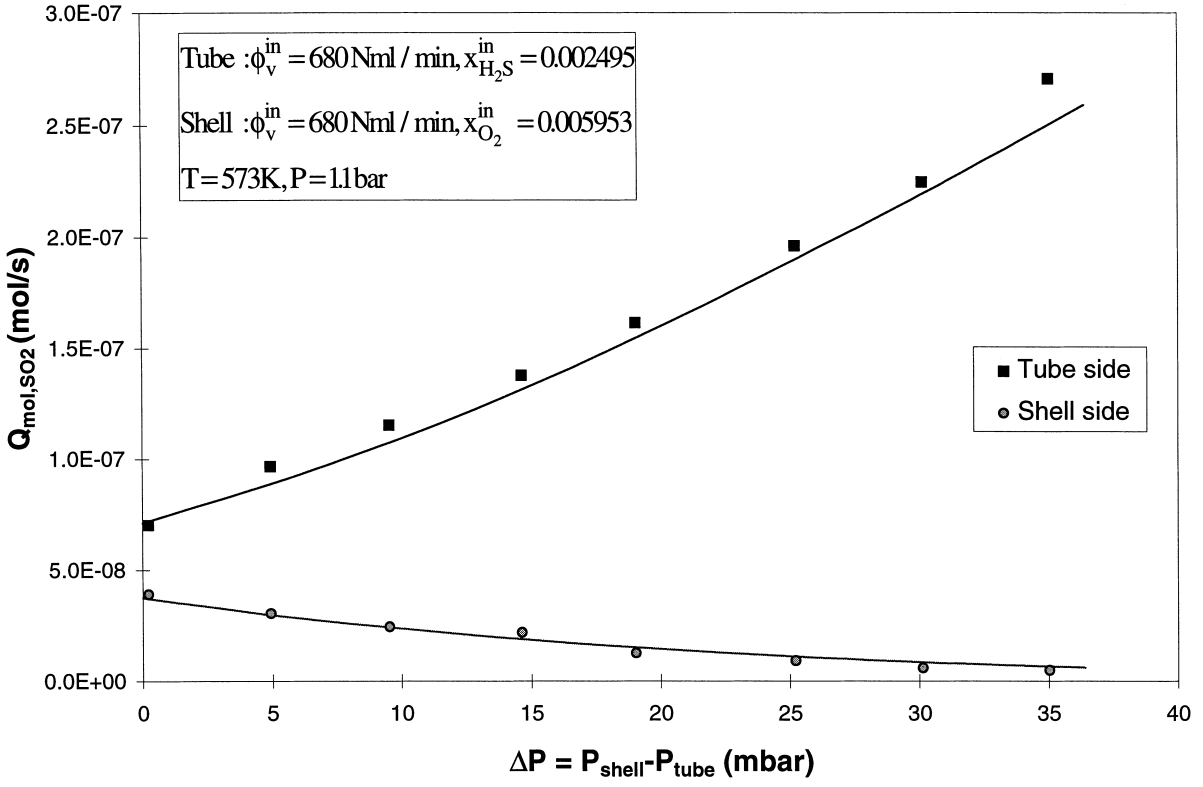

Fig. 9. Formation of SO_2 as a function of the pressure drop in tube and shell side.

activity of the construction nature of the membrane itself is used a homogeneously active membrane is guaranteed. A model based on the dusty gas model predicts the conversions in the membrane very good. The fundamental characteristics of the membrane are determined from isobaric- and permeation measurements; so no fit parameters are present in the model. The only assumption made is regarding the oxidation of H_2S as an instantaneous reaction. This study makes the conclusion justified that the fundamental description of this type of membranes can be done analogous to those of ceramic membranes, which makes the application of this membrane concept even more attractive.

7. Notation

B_0	permeation coefficient (m^2)
c	concentration (mol m^{-3})
d	diameter (m)
D	diffusion coefficient ($m^2\ s^{-1}$)
K_0	Knudsen coefficient (m)
k_r	kinetic constant (s^{-1})
k_g	mass transfer coefficient in the gas phase (m s^{-1})
r	radius (m)
L	length of membrane (m)
M	molar weight (kg mol^{-1})
N	molar flux (mol $m^{-2}\ s^{-1}$)
p	partial pressure (Pa)
P	pressure (Pa)
Q	production rate (mol s^{-1})
R	universal gas constant (J $mol^{-1}\ K^{-1}$)
T	temperature (K)
Sh	Sherwood number (dimensionless)

Greek symbols

δ_r	location of the reaction plane (m)
ϵ	porosity (dimensionless)

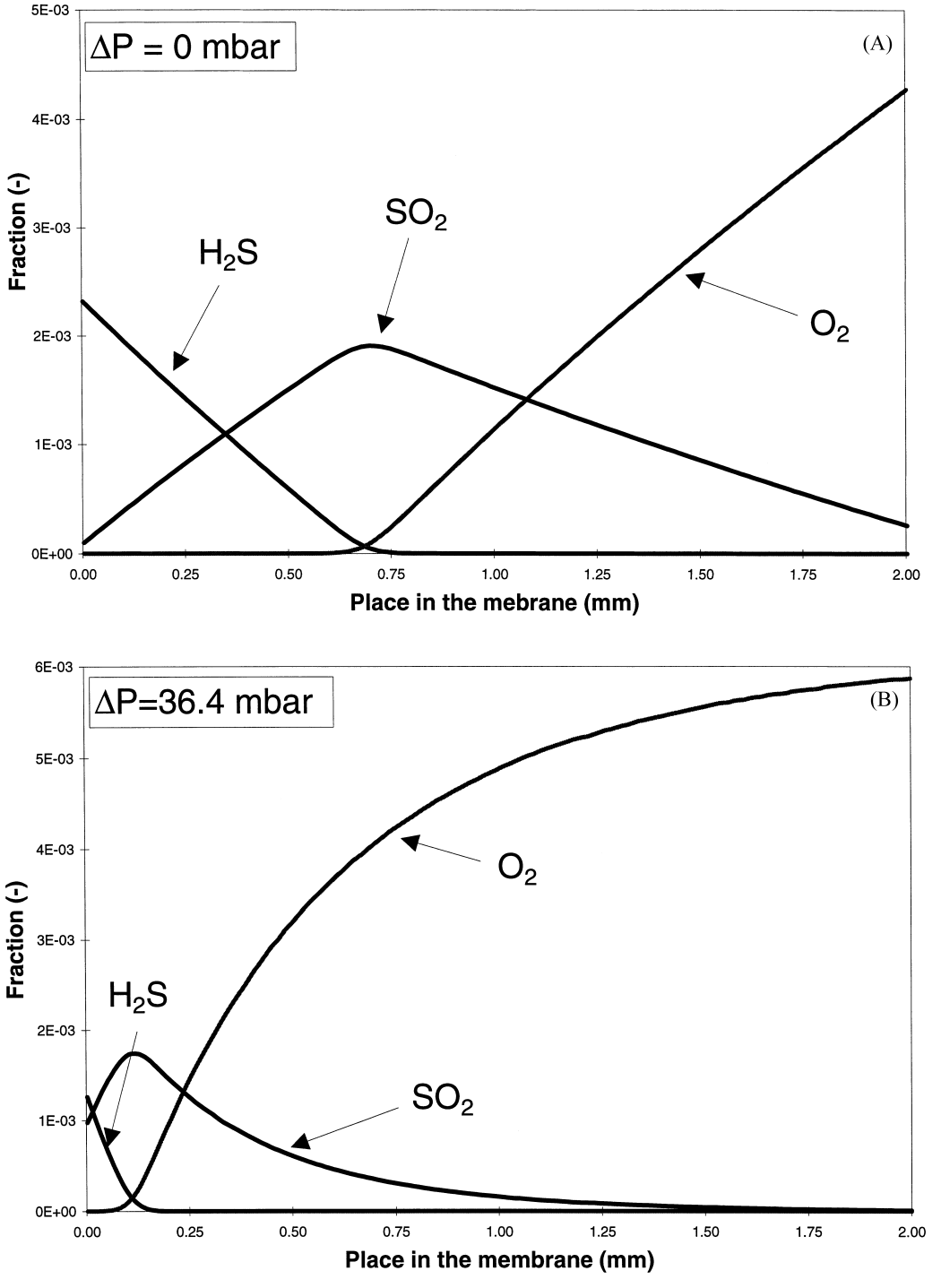

Fig. 10. (a) Fraction profile in the absence of a pressure drop; (b) Fraction profile in the presence of a pressure drop (ΔP=36.4 mbar).

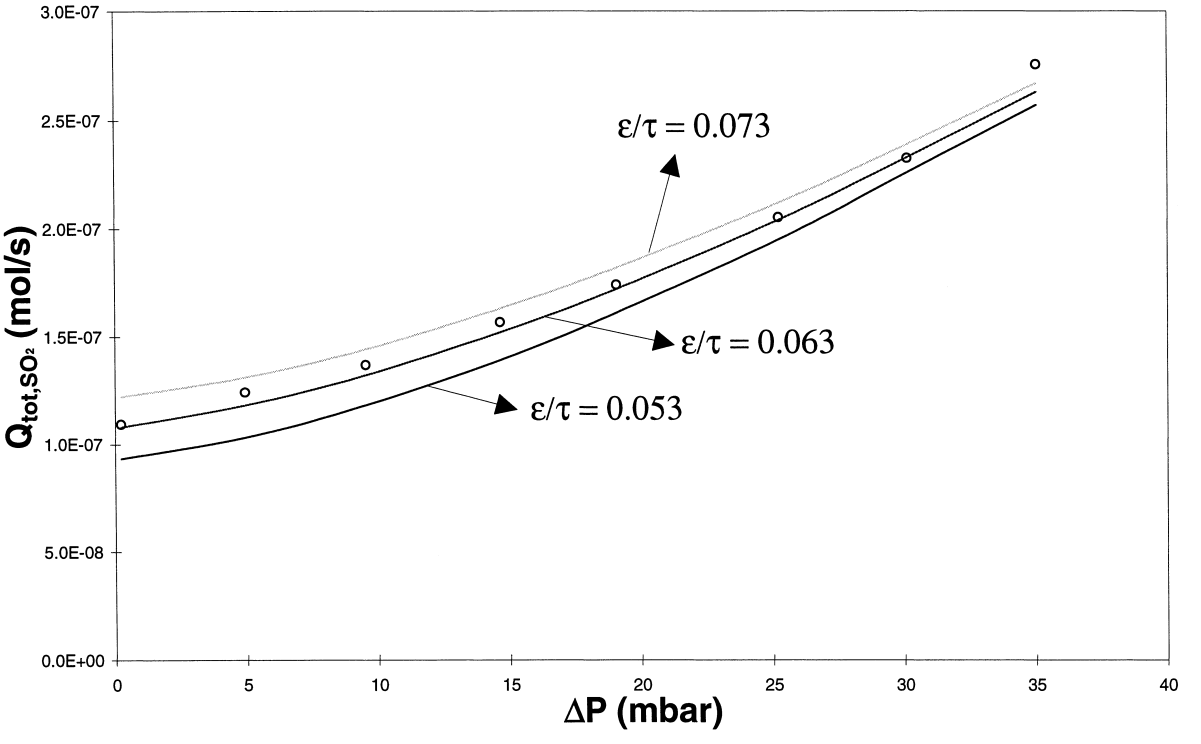

Fig. 11. Influence of ϵ/τ-ratio on total conversion of H_2S.

ϕ_{mol}	molar flow (mol s^{-1})
υ	stoichiometric constant (dimensionless)
ν_i	diffusion volume of component i (dimensionless)
τ	tortuosity (dimensionless)

Subscripts

a	for component a
b	for component b (subscript)
i	for component i
j	for component j
K	Knudsen
s	shell side
t	tube side
tot	total

Superscript

eff	effective
i	interface
s	shell side
t	tube side
0	bulk

Acknowledgements

The authors wish to thank GASTEC NV (Apeldoorn, Netherlands) for their financial support, S.C. Diender for his experimental work and H.J. Moed for his technical assistance.

References

[1] H.J. Sloot, G.F. Versteeg, W.P.M. van Swaaij, A non-permselective membrane reactor for chemical processes normally requiring strict stoichiometric feed rates of reactants, Chem. Eng. Sci. 45 (1990) 2415.

[2] J.W. Veldsink, R.M.J. van Damme, G.F. Versteeg, W.P.M. van Swaaij, A catalytically active membrane reactor for fast, heterogeneous catalysed reactions, Chem. Eng. Sci. 47(9)(11) (1992) 2939.

[3] G. Saracco, J.W. Veldsink, G.F. Versteeg, W.P.M. van Swaaij, Catalytic combustion of propane in a membrane reactor with separate feed of reactants II. Operation in presence of a trans-membrane pressure gradients, Chem. Eng. Sci. 50 (1995) 2833.

[4] J.W. Veldsink, R.M.J. van Damme, G.F. Versteeg, W.P.M. van Swaaij, The use of the dusty-gas model for the description of mass transport with chemical reaction in porous media, Chem. Eng. J. 57 (1995) 115.

[5] R.E. Lunberg, W.C. Reynolds, P.A. McCuen, Heat transfer in annular passages. Hydrodynamically developed laminar flow with arbitrarily prescribed wall temperatures or heat fluxes, Int. J. Heat Mass Transfer 6 (1963) 495.

[6] R.B. Bird, W.E. Stewart, E.N. Lightfoot, Transport Phenomena, Wiley, New York, 1960.

[7] E.N. Fuller, P.D. Schettler, J.C. Giddings, A new method for predicting of binary gas phase diffusion coefficients, Ind. Eng. Chem. 58 (1966) 18.

[8] E.A. Mason, A.P. Malinauskas, Gas Transport in Porous Media: The Dusty Gas Model, Elsevier, Amsterdam, 1983.

[9] Krebsöge product information, Filter-elements, high porous sintered materials SIKA-R. . .IS, Hofte technische agenturen B.V., Amstelveen, Netherlands, 1994.